Received: 15 May 2019 | Revised: 24 August 2019 | Accepted: 4 September 2019

DOI: 10.1002/jbm.a.36794

Society For Biomaterials WILEY

ORIGINAL ARTICLE

Sterilized chitosan-based composite hydrogels: Physicochemical characterization and in vitro cytotoxicity

Rogelio Rodríguez-Rodríguez[1] | Cristina Velasquillo-Martínez[2] | Peter Knauth[3] | Zaira López[3] | Maira Moreno-Valtierra[1] | Jorge Bravo-Madrigal[1] | Inés Jiménez-Palomar[4] | Gabriel Luna-Bárcenas[5] | Hugo Espinosa-Andrews[6] | Zaira Y. García-Carvajal[1]

[1]Biotecnología Médica y Farmacéutica, CIATEJ, Guadalajara, Jalisco, Mexico

[2]Laboratorio de Biotecnología, INR Luis Guillermo Ibarra Ibarra, Mexico City, Mexico

[3]Laboratorio de Biología Celular, CUCIÉNEGA, Universidad de Guadalajara, Ocotlán, Jalisco, Mexico

[4]inMateriis S.A. de C.V, Guadalajara, Jalisco, Mexico

[5]Departamento de Polímeros y Biopolímeros, CINVESTAV Unidad Querétaro, Querétaro, Mexico

[6]Tecnología de Alimentos, CIATEJ, Zapopan, Jalisco, Mexico

Correspondence
Zaira Y. García-Carvajal, Biotecnología Médica y Farmacéutica, CIATEJ, A.C. Av. Normalistas #800, 44270 Guadalajara, Jalisco, Mexico.
Email: zgarcia@ciatej.mx
Hugo Espinosa-Andrews, Tecnología de Alimentos, CIATEJ, A.C. Camino al Arenero #1227, 45019 Zapopan, Jalisco, Mexico.
Email: hespinosa@ciatej.mx

Funding information
Fondo Sectorial de Investigación en Salud y Seguridad Social, SSA/IMSS/ISSSTE-CONACYT, Grant/Award Number: 234073

Abstract

Gelatin/chitosan/polyvinyl alcohol hydrogels were fabricated at different polymer ratios using the freeze-drying and sterilized by steam sterilization. The thermal stability, chemical structure, morphology, surface area, mechanical properties, and biocompatibility of hydrogels were evaluated by simultaneous thermal analysis, Fourier transform infrared spectroscopy, X-ray diffraction, confocal microscopy, adsorption/desorption of nitrogen, rheometry, and 3-4,[5-dimethylthiazol-2-yl]-2,5-diphenyl tetrazolium bromide cell viability assay (MTT assay), respectively. The samples showed a decomposition onset temperature below 253.3 ± 4.8°C, a semicrystalline nature, and a highly porous structure. Hydrogels reached the maximum water uptake in phosphate-buffered saline after 80 min, showing values from nine to twelve times their dry mass. Also, hydrogels exhibiting a solid-like behavior ranging from 2,567 ± 467 to 48,705 ± 2,453 Pa at 0.1 rad/s (low frequency). The sterilized hydrogels showed low cytotoxicity (cell viability > 70%) to the HT29-MTX-E12 cell line. Sterilized hydrogels by steam sterilization can be good candidates as scaffolds for tissue engineering applications.

KEYWORDS
chitosan, hydrogels, porosity, swelling behavior, viscoelastic properties

1 | INTRODUCTION

Tissue engineering combines cells with scaffolds to restore, preserve, or enhance tissue functions as a consequence of chronic disease or trauma (Hunt, Chen, van Veen, & Bryan, 2014). Biomaterials employed as scaffolds must mimic the extracellular matrix of the native tissue providing provisional structural and mechanical support to the cells (Howard, Buttery, Shakesheff, & Roberts, 2008; Kulikouskaya et al., 2019; Liu et al., 2017; Perez-Puyana, Jiménez-Rosado, Romero, & Guerrero, 2019).

Hydrogels are biomaterials widely used for tissue engineering applications due to its biocompatibility, biodegradability, porosity, mechanical properties, water uptake without dissolution, and suitable transference of nutrients (Dziadek et al., 2019; Ullah, Othman, Javed, Ahmad, & Akil, 2015; Utech & Boccaccini, 2016). Hydrogels can be fabricated from natural polymers (e.g., gelatin, fibrin, collagen, chitosan, agar, or cellulose), or synthetic polymers (e.g., polycaprolactone, polylactic-co-glycolic acid, and polyvinyl alcohol [PVA]), depending on the properties to be promoted (Perez-Puyana, Ostos, López-Cornejo, Romero, & Guerrero, 2019). Chitosan, gelatin, and PVA are the widest polymers used in the

hydrogels fabrication; these can be combined to improve their physicochemical and biological properties (Fan, Yang, Yang, Peng, & Hu, 2016; Tsai, Hung, Lai, Wang, & Hsieh, 2014). In our previous research, gelatin/chitosan/PVA hydrogels were produced by the freeze-drying and irradiated by ultraviolet (UV) radiation. These hydrogels showed high thermal stability, high hydrophilicity, elastic properties, and biocompatibility with HT29 cells (Rodríguez-Rodríguez, García-Carvajal, Jiménez-Palomar, et al., 2019).

The sterilization methods allow obtaining hydrogels free of bacteria, yeast, and viruses (Dai, Ronholm, Tian, Sethi, & Cao, 2016). The sterilization methods approved for medical devices, including ethylene oxide (EtO), ionizing radiation (i.e., gamma and electron beam), dry heat, and steam heat (autoclaving) (International Organization for Standardization, 2009). The EtO and gamma irradiation are used in chitosan-based biomaterials; however, these can be hazardous for the operators (Ji & Shi, 2013). Besides, residual EtO is toxic, and extensive degassing is required to complete the remaining trace after the sterilization (Rediguieri, Sassonia, Dua, & Kikuchi, 2016).

The steam sterilization method is easy to use, low-cost, nontoxic, and environmentally friendly (Shamekhi et al., 2017). However, the temperature applied during steam sterilization frequently has adverse effects on the physicochemical, mechanical, and biological properties of the hydrogels (Galante et al., 2016; Yu-Min, Ya-Hong, Xiao-Hua, Fei, & Xiao-Song, 2007; Zang et al., 2014). Ji and Shi (2013) observed that steam sterilization impacted the physicochemical and mechanical properties such as porosity, swelling, compressive modulus, and biocompatibility of freeze-dried chitosan scaffolds. These results were associated with the crosslinking based amino groups induced by steam sterilization (Ji & Shi, 2013).

The purpose of this study was to produce gelatin/chitosan/PVA hydrogels sterilized by steam sterilization and to evaluate their thermal stability, chemical identity, structural morphology, size pore, surface area, swelling behavior, mechanical properties, and cytotoxicity, which have not been investigated.

2 | MATERIALS AND METHODS

2.1 | Materials

Type B gelatin (Bloom ~ 75), low molecular weight chitosan (deacetylation degree ~ 92.2%), PVA (molecular weight ~ 89 kDa and hydrolysis degree ~ 99.8%), and reagents to cytotoxicity assay were supplied from Sigma Aldrich (St. Louis, MO). All other solvents and reagents were of analytical grade.

2.2 | Preparation of polymer solutions

Gelatin solution (2.5 wt%) was prepared by dissolving gelatin powder in distilled water and gently stirred for 2 hr at 37°C. Chitosan solution (2.5 wt%) was obtained by dissolving chitosan powder in acid solution (0.4 M acetic acid solution) and gently stirred for 12 hr at 25°C. PVA solution was prepared by dissolving the powder in distilled water and gently stirred for 2 hr at 80°C.

2.3 | Fabrication of hydrogels

Hydrogels were fabricated by blending the polymer solutions at different polymer ratios according to the method previously described by Rodríguez-Rodríguez, García-Carvajal, Jiménez-Palomar, et al. (2019) (Table 1). The pH was adjusted to 4.0 to obtain homogeneous solutions.

Each blend solution was poured in plastic mold (14 ml) and frozen at −80°C for 24 hr. Then, the samples were subjected to freeze-drying using a freeze dryer (Telstar LyoQuest, Terrassa, Spain) at −80°C and to a vacuum of 0.2 mbar for 72 hr. The different samples were neutralized by sodium hydroxide solution (NaOH, 0.1 N) for 30 min. Afterward, hydrogels were put into xylene solution for 15 min to induce porosity with mechanical agitation using an orbital shaker (200 rpm) at 37°C (Espinosa-García et al., 2007; López-Velázquez et al., n.d.; Rodríguez-Rodríguez, García-Carvajal, Jiménez-Palomar, et al., 2019). The hydrogels were rinsed using a concentration gradient from ethylic alcohol from 100 to 0% to remove residual solvents. Finally, hydrogels were sterilized in phosphate-buffered saline (PBS) using a steam autoclave SE 510 (Yamato Scientific, Tokyo, Japan) at 121°C and 103.4 KPa for 15 min.

The hydrogels were freeze-dried only for thermal stability, Fourier transform spectroscopy (FTIR), X-ray diffraction (XRD), surface area analysis, and swelling test.

2.4 | Physicochemical characterization of hydrogels

2.4.1 | Thermal stability

The thermal stability of the samples in dry state was determined using a Simultaneous Thermal Analysis PT1000 thermogravimetric analysis-differential scanning calorimetry (TG-DSC) (Linseis, Selb, Germany). Dehydrated samples were ground with a grinder. Approximately 20 mg of sample was placed onto a platinum pan and heated over a temperature range from 50 to 700°C with a heating rate of 10°C/min under a nitrogen atmosphere. The temperature was calibrated using an indium standard.

2.4.2 | FTIR spectroscopy

FTIR spectroscopy was used to identify chemical changes of the samples due to the steam sterilization. The dried samples were ground with a grinder and placed on the surface of the attenuated total reflectance (ATR) of the Spectrum GX system (Perkin Elmer, Branford, CT). Spectra were obtained with a resolution of 1 cm^{-1} over 24 scans in the range from 4,000 to 650 cm^{-1}.

TABLE 1 Composition of the hydrogels at different polymer ratios

Polymer blends	Gel (2.5 wt%)	Ch (2.5 wt%)	PVA (2.5 wt%)
R1	60%	20%	20%
R2	20%	60%	20%
R3	20%	20%	60%
R4	33%	33%	33%

Abbreviation: Gel, gelatin; Ch, chitosan; PVA, polyvinyl alcohol.

2.4.3 | XRD analysis

XRD measurements of the different samples in the dry state were acquired by an X-ray diffractometer Dmax2100 (Rigaku, Tokyo, Japan) having a CuKα (λ = 0.154 nm) at a scanning speed of 10° per min over a 2θ range of 5°–40°.

2.4.4 | Morphology and surface area

The surface area of the different samples in dry state was determined by adsorption/desorption of liquid nitrogen at −196°C, using a nitrogen adsorption equipment Nova 4200e (Quantachrome Instruments, Boynton Beach, FL). First, the samples were crushed and subsequently degassed at 80°C for 12 hr. Then, the surface area of the samples (200–500 mg) was obtained from nitrogen adsorption data at relative pressures between 0.05 and 0.3 P/P_0 (equilibrium pressure and saturation pressure of adsorbates at the temperature of adsorption) using the Brunauer–Emmett–Teller (BET) multipoint method: (Sofianos et al., 2017)

$$\frac{x}{V(1-x)} = \frac{1}{(V_m)(c_{BET})} + \frac{x(c_{BET}-1)}{(V_m)(c_{BET})} \quad (1)$$

where V is the volume of adsorbed nitrogen molecules, V_m is the monolayer volume, c_{BET} is the BET constant, and x is the relative pressure (P/P_0).

The structural morphology of the hydrogels was observed by confocal microscopy DMRA2 (Leica Microsystems GmbH, Wetzlar, Germany) equipped with an Evolution QEi camera (MediaCybernetics, Bethesda, MD). Previously, hydrogels (5 mm^2) were labeled using 0.01 mg/ml rhodamine in PBS and allowed to react for 24 hr. Rhodamine B molecules were covalently conjugated with each neutral amine group of chitosan and gelatin introducing a red fluorescence. Remaining free rhodamine was taken away from the hydrogels using PBS solution. This procedure was performed while protecting the hydrogels from light exposure. Images were obtained using excitation/emission wavelengths of 530/590 and observed with ×100 magnification. The shape, geometry, and color of the hydrogels were examined by a visual check.

2.4.5 | Swelling test

The water uptake behavior of the different samples was studied using the gravimetric method. Dried samples (~200 mg) were immersed in PBS solution, taken out at different time points by 1 week, and weighed without dripping until constant mass. The percentage of water uptake in PBS medium was calculated as shown:

$$\text{Water uptake}\,(\%) = \frac{W_s - W_d}{W_d} \times 100\% \quad (2)$$

where W_s is the mass of hydrogels through time and W_d is the mass of the sample in a dry state.

2.4.6 | Rheological properties

The elastic modulus and viscous modulus of the hydrogels were obtained using an AR1000 rheometer (TA Instruments, Newcastle, DE) coupled to a cross-hatched parallel plate geometry of 40 mm with a gap of 2 mm between the flat surfaces (Rodríguez-Rodríguez, García-Carvajal, Jiménez-Palomar, et al., 2019). The oscillating sweep analysis was carried out over 0.1–100 rad/s under the linear viscoelastic region (LVER) at 20°C, where the storage modulus and loss modulus were independent of strain applied (Espinosa-Andrews et al., 2013). The elastic modulus (G', filled symbols) are shown on the left axis and viscous modulus (G'', empty symbols) are shown on the right axis. The G' and G'' values were reported on a logarithmic scale.

2.4.7 | Cytotoxicity assay

The cell viability of the different sterilized hydrogels was evaluated using extracts by 3-4,[5-dimethylthiazol-2-yl]-2,5-diphenyl tetrazolium bromide cell viability assay (MTT assay) following the ISO 10993-5:2009 standard (ISO10993-5, 1999; Rodríguez-Rodríguez, García-Carvajal, Jiménez-Palomar, et al., 2019). Hydrogels (~500 mg) were immersed in 5 ml of culture medium at 37°C for 72 hr without shaking. Then, the extracts obtained (100%) were diluted with Dulbecco's Modified Eagle Medium (DMEM) to obtain different concentrations, that is, 100, 50, 25, 12.5, and 0%. The cell line HT29-MTX-E12, a human colorectal adenocarcinoma, was cultured in DMEM medium supplemented with 10% fetal bovine serum and 1% penicillin/streptomycin. Cells were incubated until reaching ~80% confluence and seeded in a 96-well plate at 5×10^4 cells per well (37°C and 5% CO_2). The DMEM medium was removed after 24 hr and 100 μl of extracts at different concentrations (100, 50, 25, 12.5, and 0%) were added, incubating for 1, 3, and 7 days (37°C and 5% CO_2). Negative control (DMEM medium) and positive control (sodium dodecyl sulfate 1%) were used. After culture, the extracts were removed from each well, and 100 μl of MTT solution (0.5 mg/ml) was added and incubated until the formation of formazan crystals for 4 hr at 37°C. The formazan crystals were dissolved using dimethyl sulfoxide, and the absorbance was measured using a Spectrophotometer Multiskan GO (Thermo Scientific, Pittsburgh, PA) at 570 nm. The cell viability was calculated as shown:

$$\%\text{cell viability} = \frac{I_s}{I_c} \times 100 \quad (3)$$

where, I_s is the absorbance of the cells exposed to the extract and $I_c$is the absorbance of the cells nonexposed to the extract.

2.5 | Statistical analysis

All the measurements were done by triplicate and reported as means ± *SDs*. The statistical analyses were performed using a one-way analysis of variance (Statgraphics Centurion XVI version 16.1.17), and Tukey's test was used to evaluate significant differences ($p < .05$). Values with different superscript letters were significantly different ($p < .05$).

3 | RESULTS

3.1 | Thermal stability

TG-DSC analysis was used to determine the thermal processes (such as fusion or glass transition) and the mass loss of the dried samples sterilized by steam sterilization (Figure 1).

The samples displayed three events of mass loss on the TG signal between 50 and 700°C. The first thermal event was observed by a mass loss step in the TG signal and an endothermic transition of low intensity in the DSC signal between 50 and 200°C. The evaporation of residual water was found in the first thermal event: 5.6 ± 1.0^{a} % for R1, 8.5 ± 1.0^{a,b} % for R2, 10.5 ± 0.7^{b} % R3, and 10.3 ± 2.2^{b} % for R4. On the second thermal event, several exothermic peaks were observed in the DSC signal with higher mass losses in the temperature range of 200–500°C. The onset temperature decomposition founded in TG signal was 253.3 ± 4.8^{a} °C for R1, 252.7 ± 3.5^{a} °C for R2, 239.1 ± 1.9^{b} °C for R3, and 235.7 ± 3.4^{b} °C for R4. The onset temperature decomposition of R1 and R2 were significantly higher ($p < .05$) than R3 and R4 samples. On the other hand, the DSC thermograms of samples showed several broad exothermic peaks. R1, R2, and R4 samples showed four exothermic peaks, while R3 showed only three exothermic peaks. For R1, the exothermic centered peaks were observed at 299, 325, 433, and 537°C; for R2 at 297, 322, 443, and 544°C, for R3 at 292, 446, and 521°C, and R4 at 295, 326, 439, and 546°C. Finally, the third thermal even was found after 500°C.

3.2 | Fourier transform infrared spectroscopy

The FTIR spectra were obtained between 1,750 and 1,500 cm^{-1} to the dried samples sterilized by steam sterilization (SSS) and irradiated by UV radiation (SUV) (Figure 2). The amino (—NH) band was located from 1,550 to 1,570 cm^{-1}, while the carboxyl (C⍰O) band was located approximately at 1650 cm^{-1}.

The FTIR spectra of the SSS and SUV showed a similar intensity in the bands for R1 and R4. However, the strength of these bands decreased in the samples R2 and R3. The high amount of chitosan on the R2 sample shifted the amino band from 1,570 cm^{-1} in SUV sample to 1,589 cm^{-1} in SSS. This behavior did not observe in the samples with the low chitosan concentration (R1 and R3).

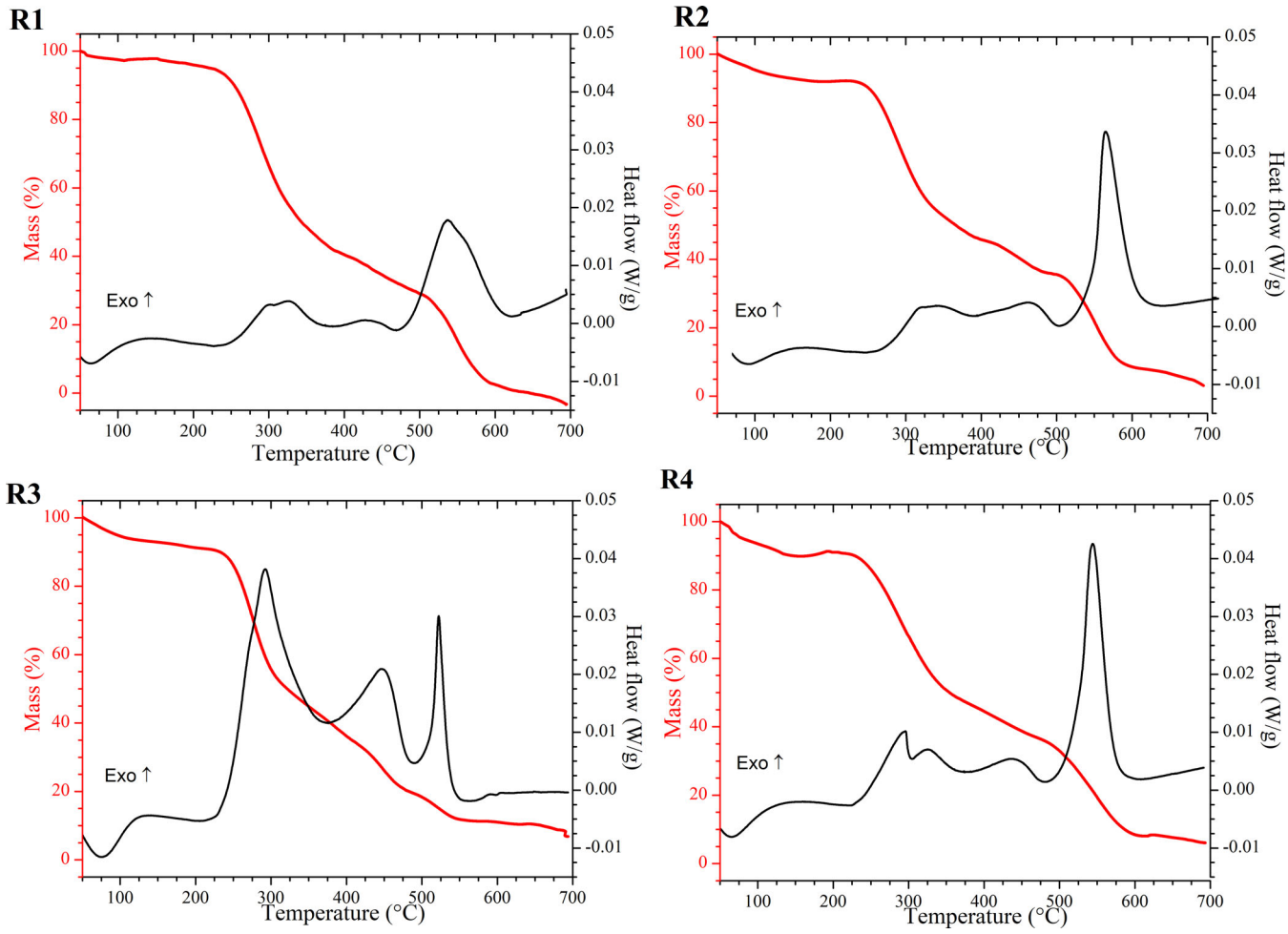

FIGURE 1 TG-DSC analysis of different gelatin/chitosan/PVA hydrogels sterilized by steam sterilization: R1, R2, R3, and R4. The change in residual mass versus temperature is shown on the left axis, and heat flow versus temperature is shown on the right axis. PVA, polyvinyl alcohol; TG-DSC, thermogravimetric analysis-differential scanning calorimetry

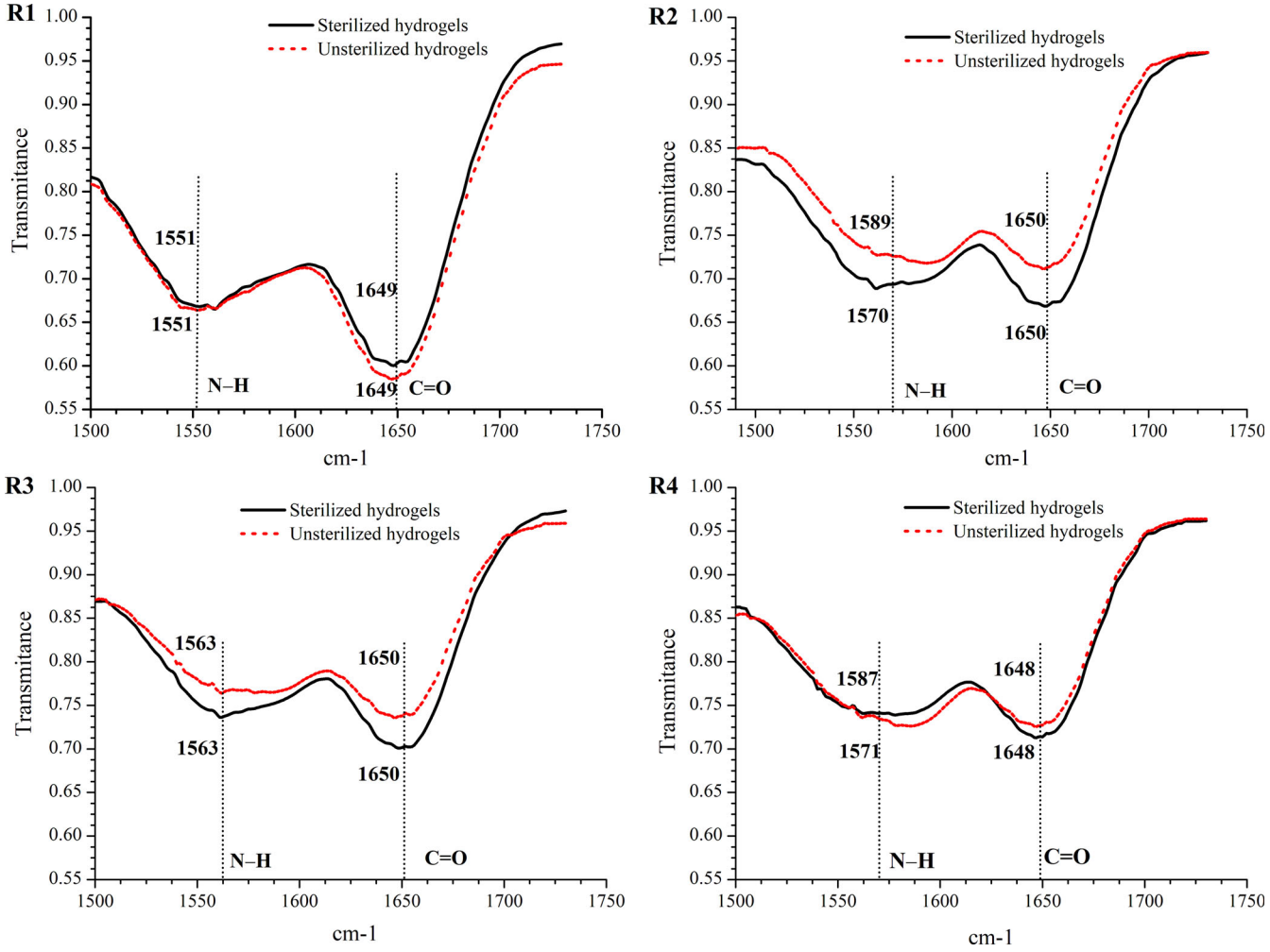

FIGURE 2 FTIR spectra of hydrogels gelatin/chitosan/PVA: R1, R2, R3, and R4 irradiated by UV radiation and sterilized by steam sterilization. The transmittance is shown on the left axis. FTIR, Fourier transform spectroscopy; PVA, polyvinyl alcohol; UV, ultraviolet

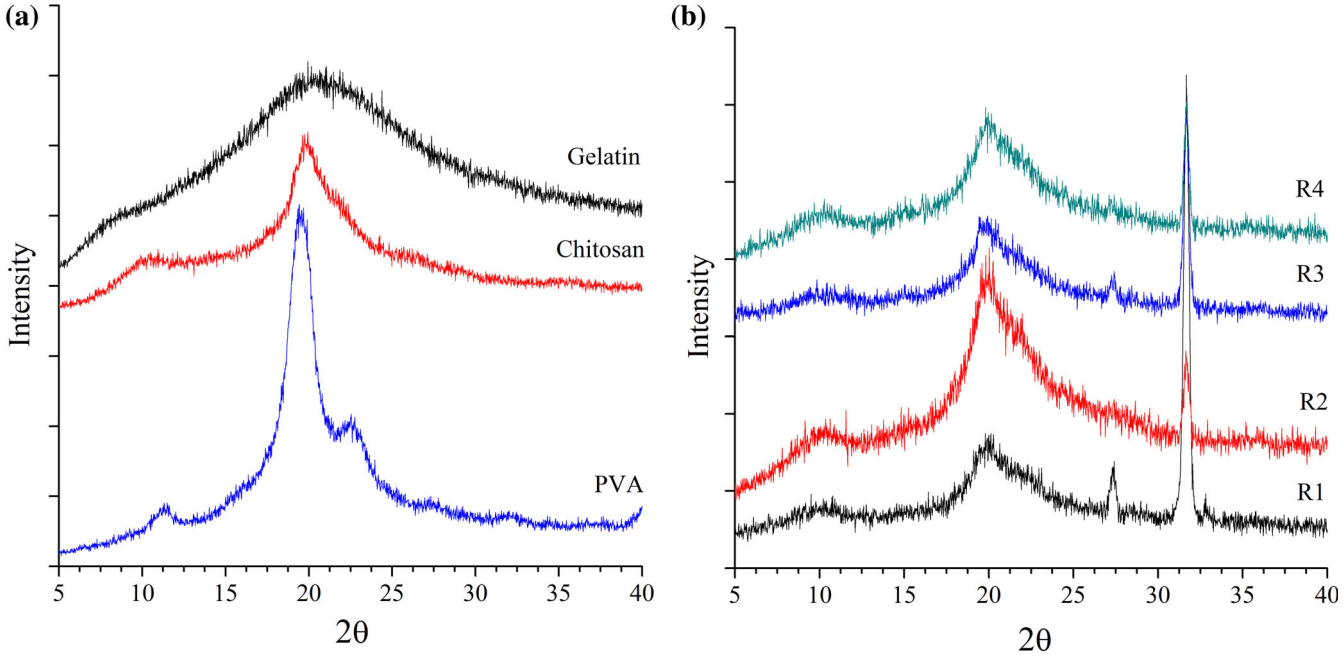

FIGURE 3 X-ray diffraction of (a) powder polymers (gelatin, chitosan, and PVA) and (b) gelatin/chitosan/PVA sterilized hydrogels by steam sterilization: R1, R2, R3, and R4. PVA, polyvinyl alcohol

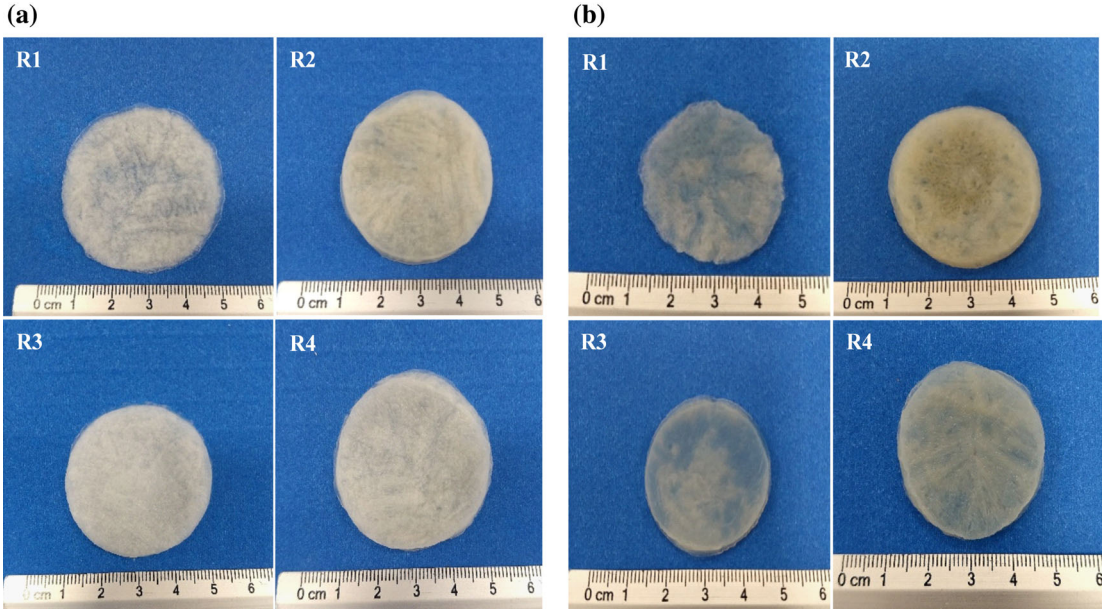

FIGURE 4 Top surface of different gelatin/chitosan/PVA samples irradiated by UV radiation (a) and sterilized by steam sterilization (b): R1, R2, R3, and R4. PVA, polyvinyl alcohol; UV, ultraviolet

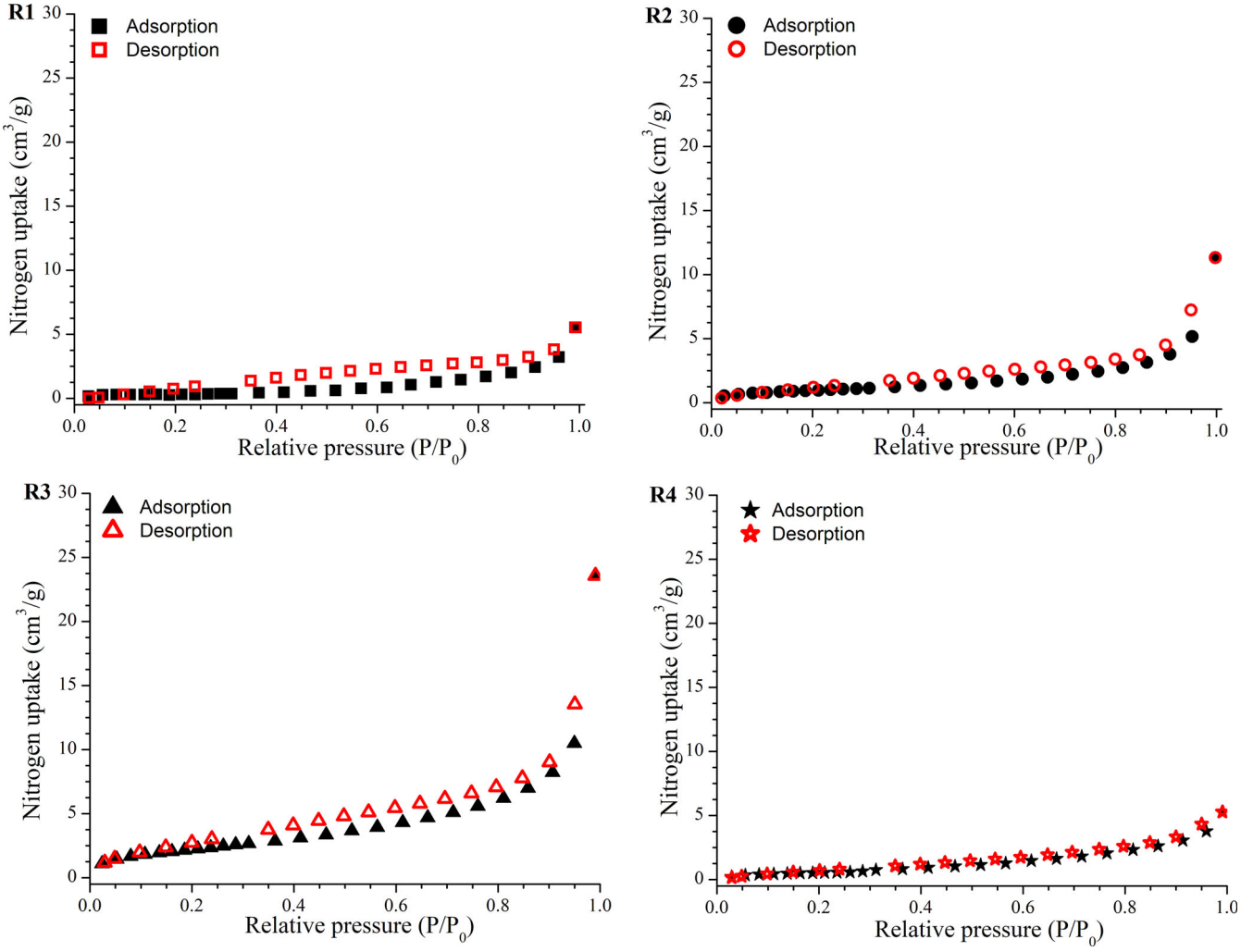

FIGURE 5 N2 adsorption–desorption isotherm of different gelatin/chitosan/PVA samples sterilized by steam sterilization: R1, R2, R3, and R4. PVA, polyvinyl alcohol

3.3 | X-ray diffraction

The Figure 3 shows the XRD patterns of polymers (gelatin, chitosan, and PVA) and dried samples sterilized by steam sterilization.

Gelatin exhibited two broad peaks; a small peak at 2θ = 8.1° and a broad peak at 2θ = 20.3°. Chitosan showed two diffraction peaks at 2θ = 10.2° and 19.8° with low intensity. PVA displayed three diffraction peaks at 2θ = 11.3°, 16.6°, and 22.6° (Figure 3a).

The samples showed four diffraction peaks (Figure 3b); a broad diffraction peak centered at 2θ = 20°, two peaks with low intensity at 2θ = 10.2°, and at 27.4°, as well as an intense peak at 2θ = 31.7°.

TABLE 2 Surface area of gelatin/chitosan/PVA samples sterilized by steam sterilization

Sample	Surface area (m^2/g)
R1	1.06 ± 0.56^{a}
R2	3.52 ± 0.22^{b}
R3	8.41 ± 1.11^{c}
R4	$2.20 \pm 1.54^{a,b}$

Note: Mean ± *SD*, $n = 3$, ^{a,b,c} same letter in the column are considered not significantly different according to Tukey HSD test ($p > .05$).
Abbreviation: PVA, polyvinyl alcohol.

3.4 | Morphology and surface area

The macroscopic appearances of hydrogels irradiated by UV radiation and sterilized by steam sterilization are shown in Figure 4.

Hydrogels showed a sponge-like structure with smooth surface topography. The hydrogels irradiated by UV showed a whitish color while hydrogels after steam sterilization showed a yellowish color, being more noticeable in R2 and R4 samples.

The nitrogen adsorption/desorption BET was carried out to determine the surface area of different dried samples sterilized by steam sterilization (Figure 5).

The samples showed a characteristic Type II isotherm International Union of Pure and Applied Chemistry classification (Sing et al., 1985), indicating reversible and unrestricted multilayer physical adsorption on macroporous solids (porous size higher than 50 nm). The samples displayed a point of inflection attributed to the formation of a monolayer (Naderi, 2015). The results showed that the surface area of samples at different polymer ratios varied from 1.06 to 8.41 m^2/g (Table 2).

The microstructure of the sterilized hydrogels by steam sterilization labeled with rhodamine B is shown in Figure 6.

The rhodamine was successfully conjugated with the amine groups of gelatin and chitosan present in the sterilized hydrogels, introducing a red fluorescence. The confocal images show hydrogels with irregular macroporous and tridimensional structures with numerous open and

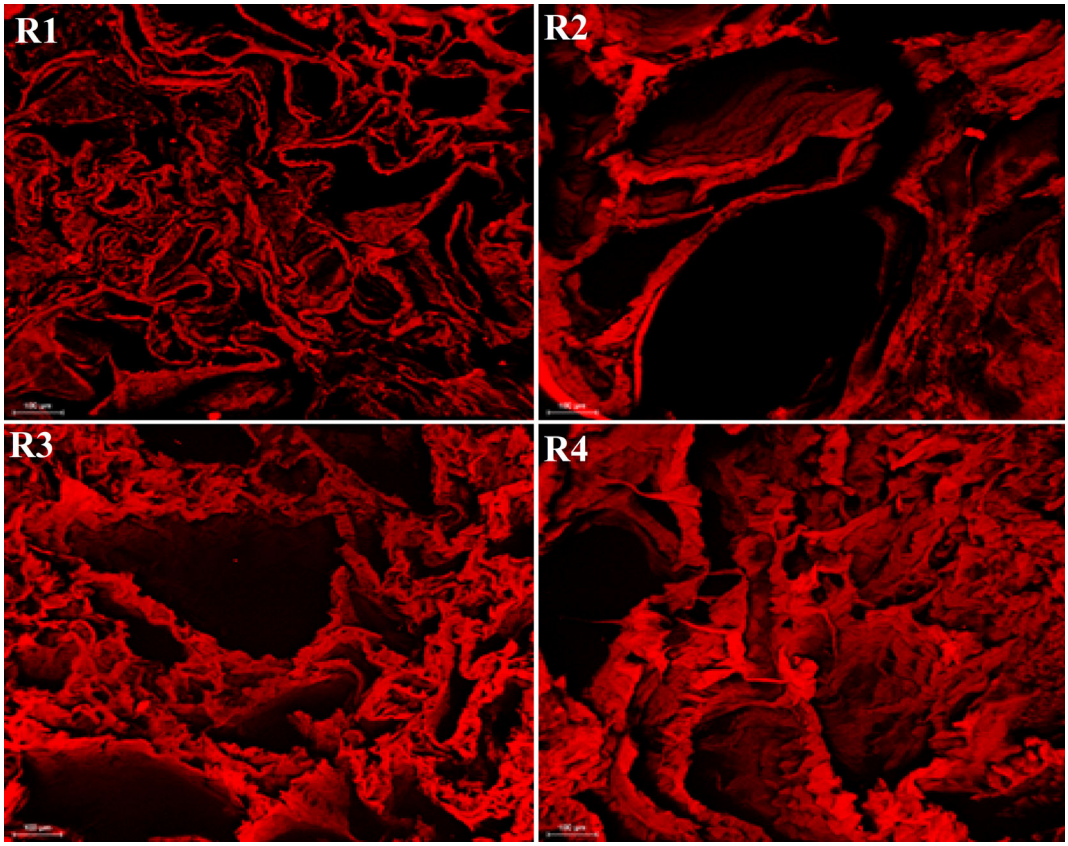

FIGURE 6 The microstructure of the hydrogels: R1, R2, R3, and R4. Samples were labeled with rhodamine B and visualized by confocal laser scanning microscopy. Red fluorescence evidenced the polymer structure of the hydrogels. (Scale bar: 100 μm)

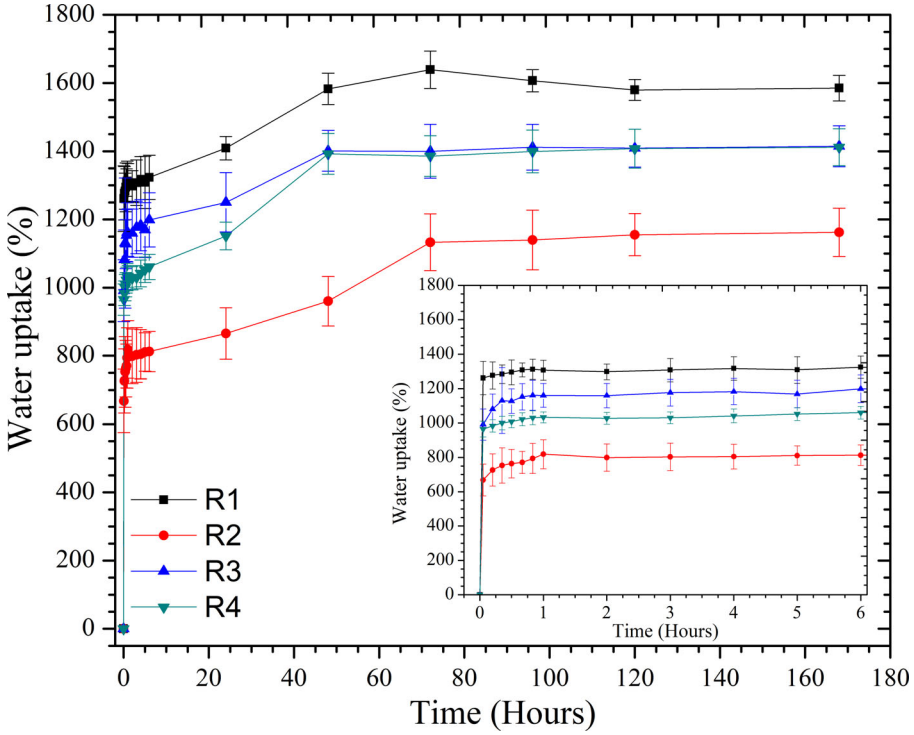

FIGURE 7 Water uptake of sterilized hydrogels as a function of time. Each point represents the mean of the results from three different samples

closed channels. Also, hydrogels displayed heterogeneous pores size with pore diameters ranging from 50 to 500 μm, where the R2 sample showed the most significant larger pore size (Figure 6).

3.5 | Swelling test

Figure 7 shows the water uptake curve of the sterilized hydrogels by steam sterilization at different time points in PBS.

The samples started swelling rapidly in the first 3 min of immersion in PBS (values from 668 ± 92.7[a] to 1,261 ± 96[b] %), reaching the maximum water uptake after 80 hr, with values from nine to twelve times their dry mass. The R1, R2, R3, and R4 samples showed maximum water uptake values of 1,585.1 ± 37.8[a], 1,161.8 ± 70.8[b], 1,414.5 ± 60.1[c], and 1,411.6 ± 54.1[c] %, respectively. The samples with higher gelatin concentration (R1) displayed the maximum value of water uptake along the time, while R2 with higher chitosan concentration had lower water uptake value. After 80 hr, the water uptake remained constant for the rest of the analysis.

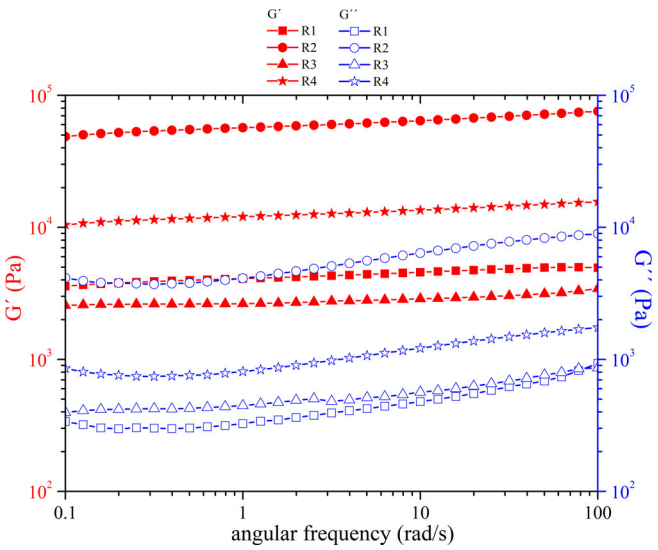

FIGURE 8 Oscillation frequency sweeps of hydrogels: [R1] (square), [R2] (circle), [R3] (triangle), and [R4] (star). The elastic modulus (*G′*, filled symbols) are shown on the left axis, and viscous modulus (*G″* empty symbols) is shown on the right axis

3.6 | Viscoelastic properties

The elastic and viscous modulus of the sterilized hydrogels by steam sterilization were obtained by oscillatory rheology to evaluate their structural differences (Figure 8).

The amplitude strain sweep results showed that the point of critical strain (i.e., the limit of the LVER where the viscoelastic properties are not strain dependent) occurred under a strain values between 2.5 and 8% (data not shown). With basis on these results, a constant strain value of 1% was selected to carry out the frequency sweeps analysis.

The hydrogels showed elastic modulus values higher than the viscous modulus, indicating that the hydrogels had a predominantly solid-viscoelastic behavior. The *G′* modulus values ranging from 2,567 to 48,705 Pa at 0.1 rad/s with the following order: R2 > R4 > R1 > R3. Moreover, R1 (3,583 ± 245[a] Pa) and R3 (2,567 ± 467[b] Pa) had the weakest mechanical properties throughout the entire frequency range, compared to hydrogels to R2 (48,705 ± 2453[c] Pa) and R4 (10,447 ± 2860[d] Pa) ($p < .05$).

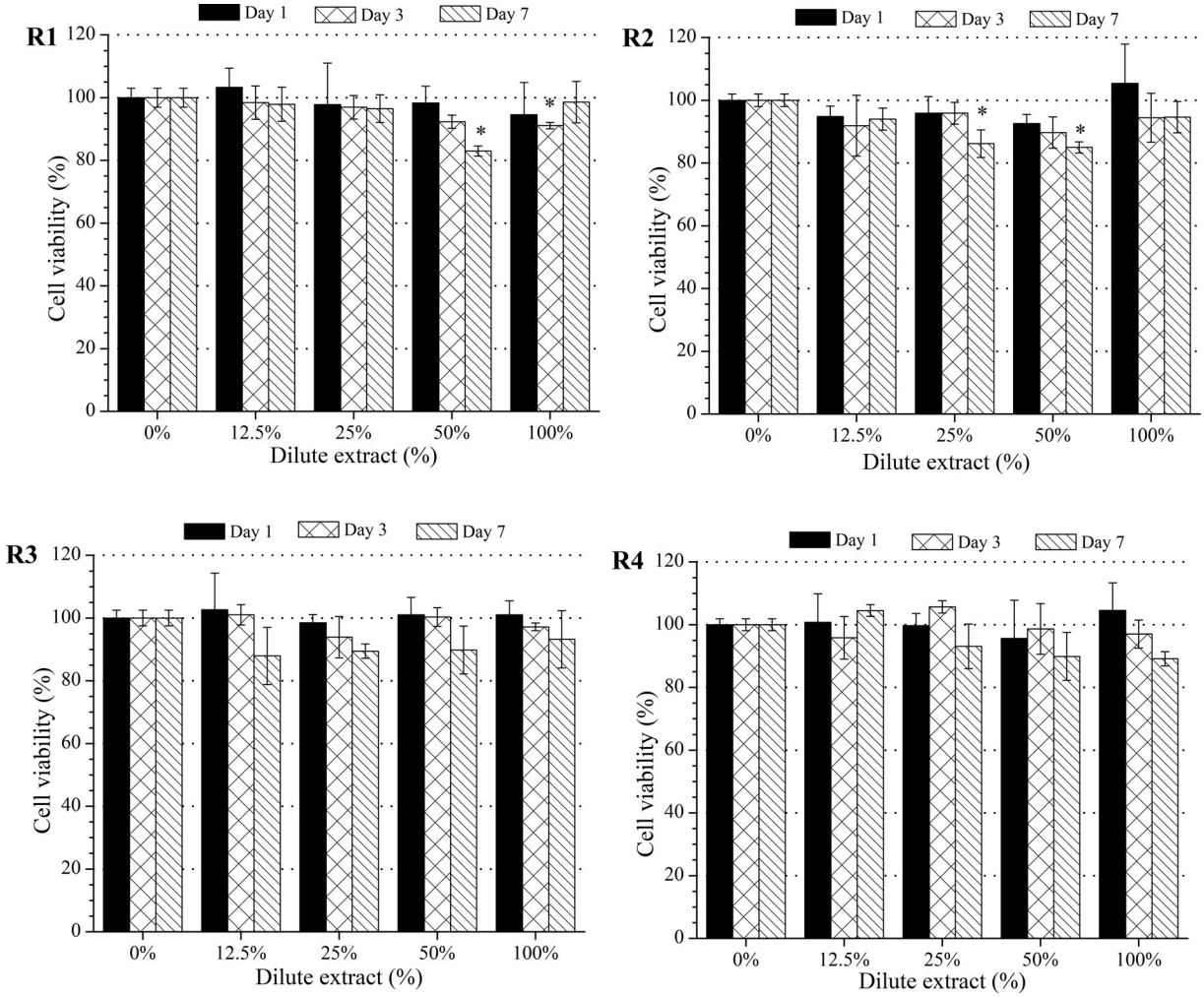

FIGURE 9 Indirect in vitro cytotoxicity of the extract medium sterilized hydrogels toward HT-29 cells by MTT assay. *Represents a significant difference compared to the control ($p < .05$)

3.7 | Cytotoxicity and cell viability

Figure 9 shows the cell viability of HT-29 cell line to the different extracts of sterilized hydrogels by steam sterilization after an incubation time of 1, 3, and 7 days.

The cell viability of the different extracts did not show statistical differences ($p < .05$) after 1 day of incubation. The cell viability was reduced after 3 and 7 days of incubation, reaching cell viability higher than 80%. The cell viability for the cells exposed to 12.5, 25, and 50% of extract medium after 3 days, as well as to 12.5 and 100% of extract medium after 7 days, did not show statistical differences ($p < .05$) independently of the polymer ratios. Besides, cells exposed to the R1 extract medium 50% and R2 extract medium with 25 and 50% decreased the cell metabolic activity after 7 days.

4 | DISCUSSION

The gelatin/chitosan/PVA hydrogels at different polymer ratios were successfully prepared and sterilized by steam sterilization.

The steam sterilization affected the thermal properties of hydrogels. TG-DSC analyses were used to know the thermal transitions involved with the mass loss and thermal transitions associated with endothermic (evaporation) or exothermic (decomposition) events (Figure 1) (Espinosa-Andrews & Rodríguez-Rodríguez, 2018; Rodríguez-Rodríguez, García-Carvajal, Jiménez-Palomar, et al., 2019). Nieto-Suárez, López-Quintela, and Lazzari (2016) suggested that water molecules are released at different temperatures intervals. Free water is eliminated between 40 and 60°C, then, water associated by H-bond is removed from 80 to 120°C, and the bound-water is removed at temperatures up to 160°C (Nieto-Suárez et al., 2016). The second thermal event was associated with the decomposition of the samples characterized by mass losses of around 48.8–54.3%. Rodríguez-Rodríguez, García-Carvajal, Jiménez-Palomar, et al. (2019) founded that gelatin/chitosan/PVA hydrogels irradiated by UV did not show statistical differences ($p < .05$) between them. However, our results showed that R1 and R2 samples had higher thermal stability than those obtained by UV radiation, while R3 and R4 did not show statistical differences ($p < .05$). Ji and Shi (2013) suggested that the steam sterilization induce the molecular interaction between the

amino groups of chitosan and gelatin and either primary hydroxyl groups or the carbonyl under high temperature, increasing the onset decomposition temperature. Finally, the exothermic peaks from the third event corresponded to the decomposition of functional groups and thermal degradation in the polymer structure of sterilized samples (Guinesi & Cavalheiro, 2006; Mullah, Joseph, Arfat, & Ahmed, 2017).

The steam sterilization induced chemical interactions in the samples, which were corroborated by FTIR analyses. Similar bands were observed in the spectra of the dried samples sterilized by steam sterilization and irradiated by UV radiation linked with the functional groups found in chitosan and gelatin (Figure 2). The shifting and changes in the intensity bands indicating chemical interactions between the functional groups present in the samples. Lim, Khor, and Ling (1999) suggested that the shift of the amino band was related to the crosslinking of the amino groups originated probably by a Millard reaction. Similarly, Ji and Shi (2013) observed the shifting of the characteristic bands from 1,637 to 1,651 cm^{-1} and 1,547 to 1,556 cm^{-1} in porous chitosan scaffolds after steam sterilization. On the other hand; sterilized hydrogels showed a yellowish color probably due to the crosslinking based on their amino groups (Figure 4) (Ji & Shi, 2013). R1 and R2 hydrogels were more yellow compared to R3 and R4 hydrogels caused by the high concentration of amino groups (Table 1).

The different gelatin/chitosan/PVA hydrogels were sterilized in PBS. The PBS is composed mainly of sodium chloride, so remaining crystals are present in the dried samples. The different samples exhibited strong reflections at $2\theta = 27.4^\circ$ and 31.7° associated with the presence of sodium chloride crystals (Bao et al., 2017). The intensity of the diffraction peaks at $2\theta = 20^\circ$ increased with increasing the chitosan concentration (R2 > R4 > R1 ≈ R3) due to encouraging the formation of crystalline regions (Figure 3b) (Costa-Júnior, Barbosa-Stancioli, Mansur, Vasconcelos, & Mansur, 2009; Islam, Riaz, & Yasin, 2013). Thein-Han, Saikhun, Pholpramoo, Misra, and Kitiyanant (2009) reported similar results in chitosan/gelatin scaffolds. They observed that the intensity of the diffraction peak at $2\theta = 20^\circ$ of chitosan decreases with increasing gelatin concentration. The crystallinity of the sample plays an essential role in the water uptake and rheology of the hydrogels (Costa-Júnior et al., 2009).

The steam sterilization exposure could have undesirable effects on the morphology and microstructure of the hydrogels. Figure 6 showed that hydrogels microstructure not collapsed. Also, the pore size was related to the surface area of the hydrogels, and the polymer ratio influenced the homogeneity and pore sizes of the samples. Ji and Shi (2013) reported that steam sterilization had no significant effect on the average pore diameter and porosity of chitosan scaffolds.

The porosity and pore size of the hydrogels are critical parameters for tissue engineering applications. Open porous and interconnected polymer structures provide adequate space for cell functions, as well as permits an appropriate transport of gases and nutrients that assure cell survival (Loh & Choong, 2013; Zeng et al., 2016). Murphy and O'Brien (2010) established that the specific surface area of the scaffolds was inversely proportional to their mean pore size. In this context, our results are directly related to the highly porous structure of the hydrogels (Kumar, Dehiya, & Sindhu, 2017; León-Mancilla, Araiza-Téllez, Flores-Flores, & Piña-Barba, 2016).

The hydrogels used as scaffolds should have optimum pore size ranges to tissue engineering applications. For example, scaffolds with pore size range from 20 to 125 μm for the regeneration of adult mammalian skin, from 150 to 200 μm for the regeneration of cartilage (Rodríguez-Rodríguez, Espinosa-Andrews, Velasquillo-Martínez, & García-Carvajal, 2019), and higher than 500 μm for adequate vascularization and survival of transplanted cells (Shoufeng, Kah-Fai, Zhaohui, & Chee-Kai, 2001).

If pores are smaller than cells, this cannot migrate through the polymer structure, as well as the diffusion of nutrients and removal of metabolic products would be limited. On the contrary, if pores are more significant than cells, the surface area decreases reducing the cell attachment (Murphy & O'Brien, 2010). Our results demonstrated that gelatin/chitosan/PVA hydrogels have appropriate pore sizes for tissue engineering applications.

The water uptake is an important issue for the diffusion of cell nutrients and the removal of metabolites through the polymer network of the hydrogels used in tissue engineering (Li & Mooney, 2016; Nieto-Suárez et al., 2016; Razavi, Qiao, & Thakor, 2019). Sterilized hydrogels displayed fast water uptake in PBS medium due to diffusion and capillary forces (Figure 7) (Peng, Peng, & Shen, 2011). The R1 sample displayed the maximum value of water uptake through all the time due to a higher hydrophilic character of gelatin compared with chitosan and PVA. The R2 sample with higher chitosan concentration had lower water uptake value, which can be related to the reduction of the electrostatic charge of the glucosamine groups (pK_a = ~6.3–7) (Rodríguez-Rodríguez, García-Carvajal, Jiménez-Palomar, et al., 2019). The swelling degree of the samples was influenced by the polymer ratio due to the amino, carboxylic, and hydroxyl groups attached to their polymer structure. In addition to the hydrophilic nature, the swelling ratio of the hydrogels was strongly influenced by their microstructure, surface area, and pore size (Yan et al., 2010). The pore size of the gelatin/chitosan/PVA sterilized hydrogels explains their high swelling degree; that is, large pore size allowed the rapid diffusion of water molecules through the hydrogel structure. Also, hydrogels with high and fast water uptake indicate the existence of inter-pore-connections in the hydrogel structure (Tripathi & Melo, 2015). When the hydrogel has contact with the water molecules, they penetrate the polymeric network and meshes extend, permitting additional water molecules to enter within the hydrogel structure (Ganji, Vasheghani-Farahani, & Ebrahim Vasheghani-Farahani, 2010).

The inflection point of the LVER corresponded to the strain necessary to breakdown the polymer structure of the sterilized hydrogels. Under this range, frequency sweep measurements affect neither the polymer structure of the hydrogel studied nor the structure formation and structure rearrangement processes (Rodríguez-Rodríguez, Espinosa-Andrews, Morales-Hernández, Lobato-Calleros, & Vernon-Carter, 2019).

The hydrogels should have adequate mechanical properties that support cell survival and functions (Liu, Smith, Hu, & Ma, 2009; Rodríguez-Rodríguez, Espinosa-Andrews, Velasquillo-Martínez, et al., 2019). The R2 hydrogel presented the higher G' modulus (48,705

± 2,453 Pa) and R3 the lower G' modulus (2,567 ± 467 Pa) (Figure 8). Rodríguez-Rodríguez, García-Carvajal, Jiménez-Palomar, et al. (2019) reported G' modulus values between 2,478 and 11,055 Pa in gelatin/chitosan/PVA hydrogels irradiated by UV radiation. These values show that the interaction between polymer chains of hydrogels irradiated was lower than the hydrogels sterilized by steam sterilization. Ji and Shi (2013) reported that steam sterilization increased the compressive modulus of chitosan scaffold from 45,500 Pa to 109,800 Pa due to the thermal-crosslinking of their polymer structure. de la Portilla et al. (2016) reported high G' modulus (1 Hz) between 6,400 and 56,600 KPa in alginate scaffolds produced with low and medium molecular weight physically crosslinked by sodium alginate and calcium gluconate. The medium molecular weight alginate and high calcium concentration produced rigid and less deformable structures, making them easier to break (de la Portilla et al., 2016). These hydrogels showed higher G' modulus than those obtained in our study due to a higher crosslinking degree.

Also, hydrogels as scaffolds should mimic the mechanical properties of native tissue, for example, cartilage has a compressive strength from 0.1 to 2.0 MPa, and spongy bone has a compressive strength from 1.9 to 7.0 MPa (Rodríguez-Rodríguez, Espinosa-Andrews, Velasquillo-Martínez, et al., 2019). Based on the mechanical properties, the gelatin/chitosan/PVA sterilized hydrogels by steam sterilization are suited for soft tissues repair or regeneration applications.

The water uptake of the sterilized hydrogels was inversely proportional to their mechanical properties. Upon swelling, the hydrogels expand their volume and deform their polymer network, decreasing their mechanical properties (Chen et al., 2016). For example, R2 hydrogel displayed the lower water uptake (1,161.8 ± 70.8%), thereby the higher elastic modulus was obtained along with the whole frequency range. Similar results were obtained by Jana, Florczyk, Leung, and Zhang (2012) using chitosan hydrogels produced by freeze-drying.

Cytotoxicity is one of the most important properties for biomaterials in tissue engineering applications. The MTT test was used to evaluate the indirect cytotoxic response to sterilized hydrogels at different polymer ratios (Carvalho & Mansur, 2017). According to ISO10993-5 (ISO10993-5, 1999), the extract medium obtained of the sterilized hydrogels does not contain toxic substances for HT29-MTX-E12 cells. Cell viability of the hydrogels was higher than 80%, indicating their good cytocompatibility. Also, comparable cell viability values were reported by Xu et al. (2017) and Ji and Shi (2013) using extracts of chitosan scaffolds sterilized by steam sterilization.

Our findings showed that all gelatin/chitosan/PVA hydrogels sterilized by steam sterilization have the potential for tissue engineering applications.

5 | CONCLUSION

In this study, gelatin/chitosan/PVA hydrogels we successfully sterilized by steam sterilization. This sterilization method modified the thermal properties, color, water uptake capacity, and viscoelastic properties of the hydrogels, where a most notorious change was displayed in the hydrogels with highest chitosan concentration. Steam sterilization induced chemical modification corroborated by FTIR and in vitro analysis showed that the different hydrogels are biocompatible and nontoxic to HT29-MTX-E12 cells.

Gelatin/chitosan/PVA hydrogels sterilized by steam sterilization have the potential for tissue engineering applications.

ACKNOWLEDGMENTS

The authors are grateful to CONACYT for the Ph.D. scholarship of M. Sc. Rogelio Rodríguez-Rodríguez. The authors are grateful to M.Sc. Reina Araceli Mauricio Sánchez (ATR-FTIR spectroscopy) and Q.A. Martín Adelaido Hernández-Landaverde (X-ray diffraction) for their technical support (CINVESTAV Unidad Querétaro). The authors also thank M.Sc. Luz María Sánchez-Noriega for their help at the Confocal Microscopy Laboratory (CIATEJ, A.C Unidad Zapopan). The authors would like to thank Ean Hundley (Peace Corps/CIATEJ) for improving the English of the manuscript.

CONFLICT OF INTEREST

The authors declare no conflict of interest.

ORCID

Rogelio Rodríguez-Rodríguez https://orcid.org/0000-0003-3383-985X
Cristina Velasquillo-Martínez https://orcid.org/0000-0002-0135-5386
Peter Knauth https://orcid.org/0000-0003-1876-4124
Zaira López https://orcid.org/0000-0003-0736-642X
Maira Moreno-Valtierra https://orcid.org/0000-0001-6156-3956
Jorge Bravo-Madrigal https://orcid.org/0000-0001-6977-9778
Inés Jiménez-Palomar https://orcid.org/0000-0002-1257-7582
Gabriel Luna-Bárcenas https://orcid.org/0000-0002-1162-6928
Hugo Espinosa-Andrews https://orcid.org/0000-0003-4635-2610
Zaira Y. García-Carvajal https://orcid.org/0000-0002-9216-0612

REFERENCES

Bao, N., Miao, X., Hu, X., Zhang, Q., Jie, X., & Zheng, X. (2017). Novel synthesis of Plasmonic Ag/AgCl@TiO2 continues Fibers with enhanced broadband Photocatalytic performance. *Catalysts*, *7*(4), 117–131.

Carvalho, I. C., & Mansur, H. S. (2017). Engineered 3D-scaffolds of photocrosslinked chitosan-gelatin hydrogel hybrids for chronic wound dressings and regeneration. *Materials Science and Engineering C*, *78*, 690–705.

Chen, H., Yang, F., Hu, R., Zhang, M., Ren, B., Gong, X., Zheng, J. (2016). A comparative study of the mechanical properties of hybrid double-network hydrogels in swollen and as-prepared states. *Journal of Materials Chemistry B*, *4*(35), 5814–5824.

Costa-Júnior, E. S., Barbosa-Stancioli, E. F., Mansur, A. A. P., Vasconcelos, W. L., & Mansur, H. S. (2009). Preparation and characterization of chitosan/poly(vinyl alcohol) chemically crosslinked blends for biomedical applications. *Carbohydrate Polymers*, *76*(3), 472–481.

Dai, Z., Ronholm, J., Tian, Y., Sethi, B., & Cao, X. (2016). Sterilization techniques for biodegradable scaffolds in tissue engineering applications. *Journal of Tissue Engineering*, *7*, 1–13.

de la Portilla, F., Pereira, S., Molero, M., De Marco, F., Perez-Puyana, V., Guerrero, A., & Romero, A. (2016). Microstructural, mechanical, and histological evaluation of modified alginate-based scaffolds. *Journal of Biomedial Materials Research Part A*, *104*(12), 3107–3114.

Dziadek, M., Kudlackova, R., Zima, A., Slosarczyk, A., Ziabka, M., Jelen, P., … Douglas, T. E. L. (2019). Novel multicomponent organic–inorganic WPI/gelatin/CaP hydrogel composites for bone tissue engineering. *Journal of Biomedical Materials Research Part A*, *107*(11), 2479–2491.

Espinosa-Andrews, H., Enríquez-Ramírez, K. E., García-Márquez, E., Ramírez-Santiago, C., Lobato-Calleros, C., & Vernon-Carter, J. (2013). Interrelationship between the zeta potential and viscoelastic properties in coacervates complexes. *Carbohydrate Polymers*, *95*(1), 161–166.

Espinosa-Andrews, H., & Rodríguez-Rodríguez, R. (2018). Water state diagram and thermal properties of fructans powders. *Journal of Thermal Analysis and Calorimetry*, *132*(1), 197–204.

Espinosa-García, B. M., Argüelles-Monal, W. M., Hernández, J., Félix-Valenzuela, L., Acosta, N., & Goycoolea, F. M. (2007). Molecularly imprinted chitosan–Genipin hydrogels with recognition capacity toward o-xylene. *Biomacromolecules*, *8*(11), 3355–3364.

Fan, L., Yang, H., Yang, J., Peng, M., & Hu, J. (2016). Preparation and characterization of chitosan/gelatin/PVA hydrogel for wound dressings. *Carbohydrate Polymers*, *146*, 427–434.

Galante, R., Rediguieri, C. F., Kikuchi, I. S., Vasquez, P. A. S., Colaço, R., Serro, A. P., & Pinto, T. J. A. (2016). About the sterilization of chitosan hydrogel nanoparticles. *PLoS One*, *11*(12), 1–18.

Ganji, F., Vasheghani-Farahani, S., & Ebrahim Vasheghani-Farahani, E. (2010). Theoretical description of hydrogel swelling: A review. *Iranian Polymer Journal*, *19*(4), 375–398.

Guinesi, L. S., & Cavalheiro, É. T. G. (2006). The use of DSC curves to determine the acetylation degree of chitin/chitosan samples. *Thermochimica Acta*, *444*(2), 128–133.

Howard, D., Buttery, L., Shakesheff, K., & Roberts, S. (2008). Tissue engineering: Strategies, stem cells and scaffolds. *Journal of Anatomy*, *213*(1), 66–72.

Hunt, J., Chen, R., van Veen, T., & Bryan, N. (2014). Hydrogels for tissue engineering and regenerative medicine. *Journal of Materials Chemistry B*, *2*(33), 5319–5338.

International Organization for Standardization. (2009). *Sterilization of medical devices. Microbiological methods. Part 2: Tests of sterility performed in the definition, validation and maintenance of a sterilization process*. ISO 11737. Switzerland.

Islam, A., Riaz, M., & Yasin, T. (2013). Structural and viscoelastic properties of chitosan-based hydrogel and its drug delivery application. *International Journal of Biological Macromolecules*, *59*, 119–124.

ISO10993-5. (1999). *Biological evaluation of medical devices-Part 5: Tests for cytotoxicity*. Geneva, Switzerland: International Organization for Standardization.

Jana, S., Florczyk, S. J., Leung, M., & Zhang, M. (2012). High-strength pristine porous chitosan scaffolds for tissue engineering. *Journal of Materials Chemistry*, *22*(13), 6291–6299.

Ji, C., & Shi, J. (2013). Thermal-crosslinked porous chitosan scaffolds for soft tissue engineering applications. *Material Science Engineering C*, *33*(7), 3780–3785.

Kulikouskaya, V., Kraskouski, A., Hileuskaya, K., Zhura, A., Tratsyak, S., & Agabekov, V. (2019). Fabrication and characterization of pectin-based 3D porous scaffolds suitable for treatment of peritoneal adhesions. *Journal of Biomedial Materials Research Part A*, *107*(8), 1814–1823.

Kumar, P., Dehiya, B. S., & Sindhu, A. (2017). Comparative study of chitosan and chitosan–gelatin scaffold for tissue engineering. *International Nano Letters*, *7*(4), 285–290.

León-Mancilla, B. H., Araiza-Téllez, M. A., Flores-Flores, J. O., & Piña-Barba, M. C. (2016). Physico-chemical characterization of collagen scaffolds for tissue engineering. *Journal of Applied Research and Technology*, *14*(1), 77–85.

Li, J., & Mooney, D. J. (2016). Designing hydrogels for controlled drug delivery. *Nature Reviews Materials*, *1*, 16071.

Lim, L.-Y., Khor, E., & Ling, C.-E. (1999). Effects of dry heat and saturated steam on the physical properties of chitosan. *Journal of Biomedical Materials Research*, *48*(2), 111–116.

Liu, M., Zeng, X., Ma, C., Yi, H., Ali, Z., Mou, X., He, N. (2017). Injectable hydrogels for cartilage and bone tissue engineering. *Bone Research*, *5*, 17014.

Liu, X., Smith, L. A., Hu, J., & Ma, P. X. (2009). Biomimetic nanofibrous gelatin/apatite composite scaffolds for bone tissue engineering. *Biomaterials*, *30*(12), 2252–2258.

Loh, Q. L., & Choong, C. (2013). Three-dimensional scaffolds for tissue engineering applications: Role of porosity and pore size. *Tissue Engineering Part B*, *19*(6), 485–502.

López-Velázquez, J. C., Rodríguez-Rodríguez, R., Espinosa-Andrews, H., Qui-Zapata, J. A., García-Morales, S., Navarro-López, D. E., García-Carvajal, Z. Y. Gelatin–chitosan–PVA hydrogels and their application in agriculture. *Journal of Chemical Technology & Biotechnology*.

Mullah, M., Joseph, L., Arfat, Y., & Ahmed, J. (2017). Thermal properties of Gelatin and chitosan. In J. Ahmed, M. Rahman, & Y. Roos (Eds.), *Glass transition and phase transitions in food and biological materials* (pp. 281–304). Chichester, England: John Wiley & Sons.

Murphy, C. M., & O'Brien, F. J. (2010). Understanding the effect of mean pore size on cell activity in collagen-glycosaminoglycan scaffolds. *Cell Adhesion & Migration*, *4*(3), 377–381.

Naderi, M. (2015). Surface area: Brunauer–Emmett–Teller (BET). In S. Tarleton (Ed.), *Progress in filtration and separation* (pp. 585–608). Oxford: Academic Press.

Nieto-Suárez, M., López-Quintela, M., & Lazzari, M. (2016). Preparation and characterization of crosslinked chitosan/gelatin scaffolds by ice segregation induced self-assembly. *Carbohydrate Polymers*, *141*, 175–183.

Peng, Z., Peng, Z., & Shen, Y. (2011). Fabrication and properties of Gelatin/chitosan composite hydrogel. *Polymer - Plastics Technology and Engineering*, *50*(11), 1160–1164.

Perez-Puyana, V., Jiménez-Rosado, M., Romero, A., & Guerrero, A. (2019). Crosslinking of hybrid scaffolds produced from collagen and chitosan. *International Journal of Biological Macromolecules*, *139*, 262–269.

Perez-Puyana, V., Ostos, F. J., López-Cornejo, P., Romero, A., & Guerrero, A. (2019). Assessment of the denaturation of collagen protein concentrates using different techniques. *Biological Chemistry*, 1–9.

Razavi, M., Qiao, Y., & Thakor, A. S. (2019). Three-dimensional cryogels for biomedical applications. *Journal of Biomedial Materials Research Part A*, 1–20.

Rediguieri, C. F., Sassonia, R. C., Dua, K., & Kikuchi, I. S. (2016). de Jesus Andreoli Pinto T. impact of sterilization methods on electrospun scaffolds for tissue engineering. *European Polymer Journal*, *82*, 181–195.

Rodríguez-Rodríguez, R., Espinosa-Andrews, H., Morales-Hernández, N., Lobato-Calleros, C., & Vernon-Carter, E. J. (2019). Mesquite gum/chitosan insoluble complexes: Relationship between the water state and viscoelastic properties. *Journal of Dispersion Science and Technology*, *40*(9), 1345–1352.

Rodríguez-Rodríguez, R., Espinosa-Andrews, H., Velasquillo-Martínez, C., & García-Carvajal, Z. Y. (2019). Composite hydrogels based on gelatin, chitosan and polyvinyl alcohol to biomedical applications: A review. *International Journal of Polymeric Materials and Polymeric Biomaterials*, 1–20.

Rodríguez-Rodríguez, R., García-Carvajal, Z., Jiménez-Palomar, I., Jiménez-Avalos, J., & Espinosa-Andrews, H. (2019). Development of gelatin/chitosan/PVA hydrogels: Thermal stability, water state, viscoelasticity, and cytotoxicity assays. *Journal of Applied Polymer Science*, *136*, 1–9.

Shamekhi, M. A., Rabiee, A., Mirzadeh, H., Mahdavi, H., Mohebbi-Kalhori, D., & Baghaban Eslaminejad, M. (2017). Fabrication and

characterization of hydrothermal cross-linked chitosan porous scaffolds for cartilage tissue engineering applications. *Materials Science and Engineering C*, *80*, 532–542.

Shoufeng, Y., Kah-Fai, L., Zhaohui, D., & Chee-Kai, C. (2001). The Design of Scaffolds for use in tissue engineering. Part I. traditional factors. *Tissue Engineering*, *7*(6), 679–689.

Sing, K. S. W., Everett, D. H., Haul, R. A. W., Mosenu, L., Pierotti, R. A., Rouquerol, J., & Siemieniewska, T. (1985). Reporting physisorption data for gas/solid systems. *Pure and Applied Chemistry*, *57*, 603–619.

Sofianos, V., Sheppard, D., Rowles, M., Humphries, T., Liu, S., & Buckley, C. (2017). Novel synthesis of porous mg scaffold as a reactive containment vessel for LiBH4. *RSC Advances*, *7*(58), 36340–36350.

Thein-Han, W., Saikhun, J., Pholpramoo, C., Misra, R., & Kitiyanant, Y. (2009). Chitosan–gelatin scaffolds for tissue engineering: Physicochemical properties and biological response of buffalo embryonic stem cells and transfectant of GFP–buffalo embryonic stem cells. *Acta Biomaterialia*, *5*(9), 3453–3466.

Tripathi, A., & Melo, J. S. (2015). Preparation of a sponge-like biocomposite agarose–chitosan scaffold with primary hepatocytes for establishing an in vitro 3D liver tissue model. *RSC Advances*, *5*(39), 30701–30710.

Tsai, R.-Y., Hung, S.-C., Lai, J.-Y., Wang, D.-M., & Hsieh, H.-J. (2014). Electrospun chitosan–gelatin–polyvinyl alcohol hybrid nanofibrous mats: Production and characterization. *Journal of the Taiwan Institute of Chemical Engineers*, *45*(4), 1975–1981.

Ullah, F., Othman, M. B. H., Javed, F., Ahmad, Z., & Akil, H. M. (2015). Classification, processing and application of hydrogels: A review. *Material Science Engineering C*, *57*, 414–433.

Utech, S., & Boccaccini, A. R. (2016). A review of hydrogel-based composites for biomedical applications: Enhancement of hydrogel properties by addition of rigid inorganic fillers. *Journal of Materials Science*, *51*(1), 271–310.

Xu, Y., Xia, D., Han, J., Yuan, S., Lin, H., & Zhao, C. (2017). Design and fabrication of porous chitosan scaffolds with tunable structures and mechanical properties. *Carbohydrate Polymers*, *177*, 210–216.

Yan, L.-P., Wang, Y.-J., Ren, L., Wu, G., Caridade, S. G., Fan, J.-B., Reis, R. L. (2010). Genipin-cross-linked collagen/chitosan biomimetic scaffolds for articular cartilage tissue engineering applications. *Journal of Biomedial Materials Research Part A*, *95A*(2), 465–475.

Yu-Min, Y., Ya-Hong, Z., Xiao-Hua, L., Fei, D., & Xiao-Song, G. (2007). The effect of different sterilization procedures on chitosan dried powder. *Journal of Applied Polymer Science*, *104*(3), 1968–1972.

Zang, S., Dong, G., Peng, B., Xu, J., Ma, Z., Wang, X., Wang, Q. (2014). A comparison of physicochemical properties of sterilized chitosan hydrogel and its applicability in a canine model of periodontal regeneration. *Carbohydrate Polymers*, *113*, 240–248.

Zeng, S., Cui, Z., Yang, Z., Si, J., Wang, Q., Wang, X., Chen, W. (2016). Characterization of highly interconnected porous poly(lactic acid) and chitosan-coated poly(lactic acid) scaffold fabricated by vacuum-assisted resin transfer molding and particle leaching. *Journal of Materials Science*, *51*(22), 9958–9970.

How to cite this article: Rodríguez-Rodríguez R, Velasquillo-Martínez C, Knauth P, et al. Sterilized chitosan-based composite hydrogels: Physicochemical characterization and in vitro cytotoxicity. *J Biomed Mater Res*. 2019;1–13. https://doi.org/10.1002/jbm.a.36794